

1 **Research article**

2 **Title**

3 Spatial variations in terrestrial net ecosystem productivity and its local indicators

4 **Running title**

5 Spatial variability in terrestrial NEP

6 **Authors**

7 Erqian Cui<sup>1,2</sup> (eqcui@stu.ecnu.edu.cn)

8 Chenyu Bian<sup>1,2</sup> (cybian@stu.ecnu.edu.cn)

9 Yiqi Luo<sup>3</sup> (yiqi.luo@nau.edu)

10 Shuli Niu<sup>4,5</sup> (sniu@igsnr.ac.cn)

11 Yingping Wang<sup>6</sup> (Yingping.Wang@csiro.au)

12 Jianyang Xia<sup>1,2,\*</sup> (jyxia@des.ecnu.edu.cn)

13 **Affiliations**

14 <sup>1</sup>Zhejiang Tiantong Forest Ecosystem National Observation and Research Station, Shanghai  
15 Key Lab for Urban Ecological Processes and Eco-Restoration, School of Ecological and  
16 Environmental Sciences, East China Normal University, Shanghai 200241, China;

17 <sup>2</sup>Research Center for Global Change and Ecological Forecasting, East China Normal University,  
18 Shanghai 200241, China;

19 <sup>3</sup>Center for ecosystem science and society, Northern Arizona University, Arizona, Flagstaff, AZ  
20 86011, USA.

21 <sup>4</sup>Key Laboratory of Ecosystem Network Observation and Modeling, Institute of Geographic  
22 Sciences and Natural Resources Research, Chinese Academy of Sciences, Beijing, China;

23 <sup>5</sup>University of Chinese Academy of Sciences, Beijing, China;

24 <sup>6</sup>CSIRO Oceans and Atmosphere, PMB 1, Aspendale, Victoria 3195, Australia.

25 **Correspondence**

26 Jianyang Xia, School of Ecological and Environmental Sciences, East China Normal University,  
27 Shanghai 200241, China.

28 Email: jyxia@des.ecnu.edu.cn

29 **Key words**

30 Net ecosystem productivity, spatial variation, net CO<sub>2</sub> uptake and release, local indicators,  
31 model

32 **Abstract**

33 Multiple lines of evidence have demonstrated the persistence of global land carbon (C) sink  
34 during the past several decades. However, both annual net ecosystem productivity (NEP) and  
35 its inter-annual variation ( $IAV_{NEP}$ ) keep varying over space. Thus, identifying local indicators  
36 for the spatially varying NEP and  $IAV_{NEP}$  is critical for locating the major and sustainable C  
37 sinks on the land. Here, based on daily NEP observations from FLUXNET sites and large-scale  
38 estimates from an atmospheric inversion product, we found a robust logarithmic correlation  
39 between annual NEP and seasonal carbon uptake-release ratio (i.e.,  $U/R$ ). The cross-site  
40 variation of mean annual NEP could be logarithmically indicated by  $U/R$ , while the spatial  
41 distribution of  $IAV_{NEP}$  was associated with the slope (i.e.,  $\beta$ ) of the logarithmic correlation  
42 between annual NEP and  $U/R$ . Among biomes, for example, forests and croplands had the largest  
43  $U/R$  ratio ( $1.06 \pm 0.83$ ) and  $\beta$  ( $473 \pm 112 \text{ g C m}^{-2} \text{ yr}^{-1}$ ), indicating the highest NEP and  $IAV_{NEP}$   
44 in forests and croplands, respectively. We further showed that these two simple indicators could  
45 directly infer the spatial variations of NEP and  $IAV_{NEP}$  in global gridded NEP products. Overall,  
46 this study provides two simple local indicators for the intricate spatial variations in the strength  
47 and stability of land C sinks. These indicators could be helpful for locating the persistent  
48 terrestrial C sinks and provides valuable constraints for improving the simulation of land-  
49 atmospheric C exchanges.

50

## 51 **1. Introduction**

52 Terrestrial ecosystems reabsorb about one-quarter of anthropogenic CO<sub>2</sub> emission (Ciais et  
53 al., 2019) and are primarily responsible for the recent temporal fluctuations of the measured  
54 atmospheric CO<sub>2</sub> growth rate (Randerson, 2013; Le Quéré et al., 2018). In addition, evidence  
55 based on eddy-flux measurements (Baldocchi et al., 2018; Rödenbeck et al., 2018), aircraft  
56 atmospheric budgets (Peylin et al., 2013), and process-based model simulations (Poulter et al.,  
57 2014; Ahlstrom et al., 2015) has shown a large spatial variability in net ecosystem productivity  
58 (NEP) on the land. The elusive variation of terrestrial NEP over space refers to both of the  
59 substantial varying mean annual NEP and the divergent inter-annual variability (IAV) in NEP  
60 (i.e., IAV<sub>NEP</sub>; usually quantified as the standard deviation of annual NEP) across space  
61 (Baldocchi et al., 2018; Marcolla et al., 2017). The mean annual NEP is related to the strength  
62 of carbon exchange of a specific ecosystem (Randerson et al., 2002; Luo and Weng, 2011; Jung  
63 et al., 2017), while IAV<sub>NEP</sub> characterizes the stability of such carbon exchange (Musavi et al.,  
64 2017). Thus, whether and how NEP and IAV<sub>NEP</sub> change over the space is important for  
65 predicting the future locations of carbon sinks on the land (Yu et al., 2014; Niu et al., 2017).

66 Large spatial difference in terrestrial NEP has been reported from eddy-flux measurements,  
67 model outputs and atmospheric inversion products. In addition, the global average IAV of NEP  
68 was large relative to global annual mean NEP (Baldocchi et al., 2018). More importantly, the  
69 spatial variations of NEP and IAV<sub>NEP</sub> were typically underestimated by the global flux tower-  
70 based product and the process-based global models (Jung et al., 2020; Fu et al., 2019). These  
71 discrepancies further revealed the necessary to identify local indicators for the spatially varying  
72 NEP and IAV<sub>NEP</sub>, separately. The NEP in terrestrial ecosystems is determined by two  
73 components, including vegetation photosynthesis and ecosystem respiration (Reichstein et al.,  
74 2005), and their relative difference could determine the spatial variation of NEP (Baldocchi et  
75 al., 2015; Biederman et al., 2016). Many previous analyses have attributed the IAV<sub>NEP</sub> at the site  
76 level to the different sensitivities of ecosystem photosynthesis and respiration to environmental  
77 drivers (Gilmanov et al., 2005; Reichstein et al., 2005) and biotic controls (Besnard et al., 2018;  
78 Musavi et al., 2017). For example, some studies have reported that IAV<sub>NEP</sub> is more associated  
79 with variations in photosynthesis than carbon release (Ahlstrom et al., 2015; Novick et al., 2015;

80 Li et al., 2017), whereas others have indicated that respiration is more sensitive to anomalous  
81 climate variability (Valentini et al., 2000; von Buttlar et al., 2017). However, despite the previous  
82 efforts in a predictive understanding of the land-atmospheric C exchanges, the multi-model  
83 spread has not reduced over time (Arora et al., 2019). Therefore, it is imperative to explore the  
84 potential indicators for the spatially varying NEP, which could help attribute the spatial variation  
85 of NEP and  $IAV_{NEP}$  into different processes and provide valuable constraints for the global C  
86 cycle. Alternatively, the annual NEP of a given ecosystem can be also directly decomposed into  
87 net CO<sub>2</sub> uptake flux and CO<sub>2</sub> release flux (Gray et al., 2014), which are more direct components  
88 for NEP (Fu et al., 2019). It is still unclear how the ecosystem net CO<sub>2</sub> uptake and release fluxes  
89 would control the spatially varying NEP.

90 Conceptually, the total net CO<sub>2</sub> uptake flux ( $U$ ) is determined by the length of CO<sub>2</sub> uptake  
91 period ( $CUP$ ) and the CO<sub>2</sub> uptake rate, while the total net CO<sub>2</sub> release flux ( $R$ ) depends on the  
92 length of CO<sub>2</sub> release period ( $CRP$ ) and the CO<sub>2</sub> release rate (Fig. 1b). The variations of NEP  
93 thus could be attributed to these decomposed components. A strong spatial correlation between  
94 mean annual NEP and length of CO<sub>2</sub> uptake period has been reported in evergreen needle- and  
95 broad-leaved forests (Churkina et al., 2005; Richardson et al., 2013; Keenan et al., 2014),  
96 whereas atmospheric inversion data and vegetation photosynthesis model indicated a dominant  
97 role of the maximal carbon uptake rate (Fu et al., 2017; Zhou et al., 2017). However, the relative  
98 importance of these phenological and physiological indicators for the spatially varying NEP  
99 remains unclear.

100 In this study, we decomposed annual NEP into  $U$  and  $R$ , and explored the local indicators  
101 for spatially varying NEP. Based on the eddy-covariance fluxes from FLUXNET2015 Dataset  
102 (Pastorello et al., 2017) and the atmospheric inversion product (Rödenbeck et al., 2018), we  
103 examined the relationship between NEP and its direct components. In addition, we used the  
104 observations to evaluate the spatial variations of NEP and  $IAV_{NEP}$  in the FLUXCOM product  
105 and a process-based model (CLM4.5) (Oleson et al., 2013). The major aim of this study is to  
106 explore whether there are useful local indicators for the spatially varying NEP and  $IAV_{NEP}$  in  
107 terrestrial ecosystems.

## 108 **2. Materials and Methods**

## 109 **2.1 Datasets**

110 Daily NEP observations of eddy covariance sites are obtained from the FLUXNET2015 Tier 1  
111 dataset (<http://fluxnet.fluxdata.org/data/fluxnet2015-dataset/>). The FLUXNET2015 dataset  
112 provides half-hourly data of carbon, water and energy fluxes at over 210 sites that are  
113 standardized and gap-filled (Pastorello et al., 2017). However, time series of most sites are still  
114 too short for the analysis of inter-annual variation in NEP. So only the sites that provided the  
115 availability of eddy covariance flux measurements for at least 5 years are selected. This leads to  
116 a global dataset of 72 sites with different biomes across different climatic regions. Based on the  
117 biome classification from the International Geosphere-Biosphere Programme (IGBP) provided  
118 for the FLUXNET2015 sites, the selected sites include 35 forests (FOR), 15 grasslands (GRA),  
119 11 croplands (CRO), 4 wetlands (WET), 2 shrublands (SHR) and 5 savannas (SAV) (Fig. S1  
120 and Table S1).

121 The Jena CarboScope Inversion product compiles from high precision measurements of  
122 atmospheric CO<sub>2</sub> concentration with simulated atmospheric transport to infer the net CO<sub>2</sub>  
123 exchanges between land, ocean and atmosphere at large scales (Rödenbeck et al., 2018). Here,  
124 we used the daily land-atmosphere CO<sub>2</sub> fluxes from the s85\_v4.1 version at a spatial resolution  
125 of 5° × 3.75°. Considering the relatively low spatial resolution of the Jena Inversion product, the  
126 daily fluxes were only used to calculate the local indicators for the spatially varying NEP at the  
127 global scale.

128 Daily NEP simulations from Community Land Model version 4.5 (CLM4.5) were also used  
129 to calculate the local indicators for the spatially varying NEP at the corresponding flux tower  
130 sites. We ran the CLM4.5 model from 1985 to 2010 at a spatial resolution of 1° with CRUNECF  
131 meteorological forcing. Here, NEP was derived as the difference between GPP and TER, and  
132 TER was calculated as the sum of simulated autotrophic and heterotrophic respiration. The daily  
133 outputs from CLM4.5 were used to calculate the local indicators for the spatially varying NEP  
134 both at the global scale and at the FLUXNET site level.

135 The FLUXCOM product presents an upscaling of carbon flux estimates from 224 flux  
136 tower sites based on multiple machine learning algorithms and meteorological drivers (Jung et  
137 al., 2017). To be consistent with the meteorological forcing of Jena Inversion product and the

138 CLM4.5 model, we used the FLUXCOM CRUNCEPv6 products. In addition, in order to reduce  
 139 the uncertainty caused by machine-learning methods, we averaged all the FLUXCOM  
 140 CRUNCEPv6 products with different machine-learning methods. It should be noted that the  
 141 inter-annual variability of FLUXCOM product is driven by meteorological measurements and  
 142 satellite data, which partially includes information on vegetation state and other land surface  
 143 properties. The FLUXCOM NEP product is downloaded from the Data Portal of the Max Planck  
 144 Institute for Biochemistry (<https://www.bgc-jena.mpg.de/geodb/projects/Home.php>). Daily  
 145 outputs from FLUXCOM for the period 1985-2010 at 0.5° spatial resolution were used to  
 146 calculate the local indicators for the spatially varying NEP both at the global scale and at the  
 147 FLUXNET site level.

## 148 **2.2 Decomposition of NEP and the calculations for its local indicators**

149 The annual NEP of a given ecosystem can be defined numerically as the difference between the  
 150 net CO<sub>2</sub> uptake and release (Figure 2b). These components of NEP contain both photosynthesis  
 151 and respiration flux, which directly indicate the net CO<sub>2</sub> exchange of an ecosystem. The total  
 152 net CO<sub>2</sub> uptake flux ( $U$ ) and the total net CO<sub>2</sub> release flux ( $R$ ) can be further decomposed as:

$$153 \quad U = \bar{U} \times CUP \quad (1)$$

$$154 \quad R = \bar{R} \times CRP \quad (2)$$

155 where  $CUP$  (d yr<sup>-1</sup>) is the length of CO<sub>2</sub> uptake period and  $CRP$  (d yr<sup>-1</sup>) is the length of CO<sub>2</sub>  
 156 release period;  $\bar{U}$  (g C m<sup>-2</sup> d<sup>-1</sup>) is the mean daily net CO<sub>2</sub> uptake over  $CUP$  and  $\bar{R}$  (g C m<sup>-2</sup> d<sup>-1</sup>)  
 157 represents the mean daily net CO<sub>2</sub> release over  $CRP$ . Many studies have reported that the  
 158 vegetation net CO<sub>2</sub> uptake during the growing season and the non-growing season soil net CO<sub>2</sub>  
 159 release are tightly correlated (Luo et al., 2014; Zhao et al., 2016). Therefore, we further tested  
 160 the relationship between annual NEP and  $\frac{U}{R}$  (i.e.,  $NEP \propto \frac{U}{R}$ ), which reflects the seasonal  
 161 carbon uptake-release ratio. Consequently, NEP in any given ecosystem can be expressed as  
 162 (Fig. S2):

$$163 \quad NEP = \beta \cdot \ln\left(\frac{U}{R}\right) \quad (3)$$

164 where the parameter  $\beta$  represents the slope of the linear relationship of  $NEP \propto \ln\left(\frac{U}{R}\right)$ ,  
165 indicating the site-level carbon uptake sensitivity. Based on the definitions of  $U$  and  $R$ , the ratio  
166  $\frac{U}{R}$  can be further written as:

$$167 \quad \frac{U}{R} = \frac{\bar{U}}{\bar{R}} \cdot \frac{CUP}{CRP} \quad (4)$$

168 Ecologically, the ratio of  $\frac{\bar{U}}{\bar{R}}$  reflects the relative physiological difference between  
169 ecosystem  $CO_2$  uptake and release strength, while the ratio of  $\frac{CUP}{CRP}$  is an indicator of net  
170 ecosystem  $CO_2$  exchange phenology. Environmental changes may regulate these ecological  
171 processes and ultimately affect the ecosystem NEP. The slope  $\beta$  indicates the response sensitivity  
172 of NEP to the changes in phenology and physiological processes. All of  $\beta$ ,  $\frac{CUP}{CRP}$  and  $\frac{\bar{U}}{\bar{R}}$  were  
173 then calculated from the selected eddy covariance sites and the corresponding pixels of these  
174 sites in models. These derived indicators from eddy covariance sites were then used to  
175 benchmark the results extracted from the same locations in models.

## 176 2.4 Calculation of the relative contributions

177 We further quantified the relative contributions of  $\frac{\bar{U}}{\bar{R}}$  and  $\frac{CUP}{CRP}$  in driving the spatial variations  
178 in NEP:

$$179 \quad NEP = \beta \cdot \left[ \ln\left(\frac{\bar{U}}{\bar{R}}\right) + \ln\left(\frac{CUP}{CRP}\right) \right] \quad (5)$$

180 For a specific ecosystem, the parameter  $\beta$  was constant. Then, we used a relative  
181 importance analysis method to quantify the relative contributions of these two ratios to the  
182 spatial variations in NEP. The algorithm was performed with the “ralaimpo” package in R (R  
183 Development Core Team, 2011). The “relaimpo” package is based on variance decomposition  
184 for multiple linear regression models. We chose the most commonly used method named  
185 “Lindeman-Merenda-Gold (LMG)” (Grömping, 2007) from the methods provided by the  
186 “ralaimpo” package. This method allows us to quantify the contributions of explanatory  
187 variables in a multiple linear regression model. Across the 72 FLUXNET sites, we quantified  
188 the relative importance of  $\frac{\bar{U}}{\bar{R}}$  and  $\frac{CUP}{CRP}$  to cross-site changes in NEP.

## 189 3. Results

### 190 3.1 The relationship between NEP and its direct components

191 To find local indicators for the spatially varying NEP in terrestrial ecosystems, we tested the  
192 relationship between NEP and its direct components ( $U$  and  $R$ ) across the 72 flux-tower sites.  
193 The results showed that annual NEP was closely related with the ratio of  $\frac{U}{R}$  (Fig. S2). The  
194 logarithmic correlations between annual NEP and  $\frac{U}{R}$  were significant at all sites (Fig. 1a), and  
195 ~90% of  $R^2$  falling within a range from 0.7 to 1 (Fig. 1c).

196 In addition, the relationship between NEP and  $\frac{U}{R}$  was also confirmed by the atmospheric  
197 inversion product (i.e., Jena CarboScope Inversion). The control of  $\frac{U}{R}$  on annual NEP was  
198 robust in most global grid cells (i.e.  $0.6 < R^2 < 1$ ). The explanation of  $\frac{U}{R}$  was higher in 80% of  
199 the regions, but lower in North American (Fig. 2). These two datasets both showed that the  
200 indicator  $\frac{U}{R}$  could successfully capture the variability in annual NEP.

### 201 3.2 Local indicators for spatially varying NEP

202 Across the 72 flux-tower sites, the across-site variation in mean annual NEP were significantly  
203 correlated to mean annual  $\ln\left(\frac{U}{R}\right)$  of each site ( $R^2 = 0.65$ ,  $P < 0.01$ ) (Fig. 3a). This finding  
204 suggested that the mean annual ratio  $\ln\left(\frac{U}{R}\right)$  is a good indicator for cross-site variation in NEP.  
205 By contrast, the spatial variation of  $IAV_{NEP}$  was moderately explained by the slope (i.e.,  $\beta$ ) of  
206 the temporal correlation between NEP and  $\ln\left(\frac{U}{R}\right)$  at each site ( $R^2 = 0.39$ ,  $P < 0.01$ ; Fig. 3b)  
207 rather than  $\ln\left(\frac{U}{R}\right)$  (Fig. S3). The wide range of ratio  $\beta$  reveals a large divergence of NEP  
208 sensitivity across biomes, ranging from  $121 \pm 118 \text{ g C m}^{-2} \text{ yr}^{-1}$  in shrubland to  $473 \pm 112 \text{ g C m}^{-2}$   
209  $\text{yr}^{-1}$  in cropland.

210 The decomposition of indicator  $\frac{U}{R}$  into  $\frac{\bar{U}}{\bar{R}}$  and  $\frac{CUP}{CRP}$  allowed us to quantify the relative  
211 importance of these two ratios in driving NEP variability. The linear regression and relative  
212 importance analysis showed a more important role of  $\frac{CUP}{CRP}$  (58%) than  $\frac{\bar{U}}{\bar{R}}$  (42%) in explaining



213 the cross-site variation of NEP (Fig. 4). Therefore, the spatial distribution of mean annual NEP  
214 was more strongly driven by the phenological changes.

### 215 **3.3 Simulated spatial variations in NEP by models**

216 We further used these two simple indicators (i.e.,  $\frac{U}{R}$  and  $\beta$ ) to evaluate the simulated spatial  
217 variations of NEP by the global flux tower-based product (i.e., FLUXCOM) and a widely-used  
218 process-based model at the FLUXNET site level (i.e., CLM4.5). We found that the low spatial  
219 variation of mean annual NEP in FLUXCOM and CLM4.5 could be inferred from their more  
220 converging  $\ln\left(\frac{U}{R}\right)$  than flux-tower measurements (Fig. 5). The underestimated variation of  
221  $IAV_{NEP}$  in these modeling results was also clearly shown by the smaller  $\beta$  values (268.22, 126.00  
222 and 145.08 for FLUXNET, FLUXCOM and CLM4.5, respectively) (Fig. 5b).

223 In addition, the spatial variations of NEP and  $IAV_{NEP}$  were associated with the spatial  
224 resolution of the product (Marcolla et al., 2017). Considering the scale mismatch between  
225 FLUXNET sites and the gridded product, we run the same analysis at the global scale based on  
226 Jena Inversion product. At the global scale, the spatial variation of mean annual NEP can be also  
227 well indicated by  $\ln\left(\frac{U}{R}\right)$  (Fig. 6). The larger net C uptake in FLUXCOM resulted from its  
228 higher simulations for  $\ln\left(\frac{U}{R}\right)$ . Furthermore, the larger spatial variation of  $IAV_{NEP}$  in CLM4.5  
229 could be inferred from the indicator  $\beta$ .

## 230 **4. Discussion**

### 231 **4.1 New perspective for locating the major and sustainable land C sinks**

232 Large spatial differences of mean annual NEP and  $IAV_{NEP}$  have been well-documented in  
233 previous studies (Jung et al., 2017; Marcolla et al., 2017; Fu et al., 2019). Here we provide a  
234 new perspective for quantifying the spatially varying NEP by tracing annual NEP into several  
235 local indicators. Therefore, these traceable indicators could provide useful constraints for  
236 predicting annual NEP, especially in areas without eddy-covariance towers.

237 Typically, the C sink capacity and its stability of a specific ecosystem are characterized  
238 separately (Keenan et al., 2014; Ahlstrom et al., 2015; Jung et al., 2017). Here we integrated

239 NEP into two simple indicators that could directly locate the major and sustainable land C sink.  
240 Among biomes, forests and croplands had the largest  $\ln\left(\frac{U}{R}\right)$  and  $\beta$ , indicating the strongest and  
241 the most unstable C sink in forests and croplands, respectively. However, the relatively lower  $\beta$   
242 in shrublands and savannas should be interpreted cautiously. There are very few semi-arid  
243 ecosystems in the FLUXNET sites, while they represent a large portion of land at the global  
244 scale and have been shown to substantially control the interannual variability of NEP (Ahlström  
245 et al., 2015). The highest  $\beta$  implies that the land covered by cropland with the largest  $\text{IAV}_{\text{NEP}}$ .  
246 Therefore, the reported rapid global expansion of cropland may enlarge the fluctuations in Land-  
247 atmosphere  $\text{CO}_2$  exchange. In fact, the cropland expansion has been confirmed as one important  
248 driver of the recent increasing global vegetation growth peak (Huang et al., 2018) and  
249 atmospheric  $\text{CO}_2$  seasonal amplitude (Gary et al., 2014; Zeng et al., 2014).

#### 250 **4.2 Joint control of plant phenology and physiology on mean annual NEP**

251 Recent studies have demonstrated that the spatiotemporal variations in terrestrial gross primary  
252 productivity are jointly controlled by plant phenology and physiology (Xia et al., 2015; Zhou et  
253 al., 2016). Here we demonstrated that the spatial difference of mean annual NEP was determined  
254 by both the phenology indicator  $\frac{\text{CUP}}{\text{CRP}}$  (58%) and the physiological indicator  $\frac{\bar{U}}{\bar{R}}$  (42%). In  
255 addition, the lower contribution of the physiological indicator could partly be attributed to the  
256 convergence of  $\frac{\bar{U}}{\bar{R}}$  across FLUXNET sites (Fig. S4).

257 The convergent  $\frac{\bar{U}}{\bar{R}}$  across sites was first discovered by Churkina *et al.* (2005) as  $2.73 \pm 1.08$   
258 across 28 sites, which included DBF, EBF and crop/grass. In this study, we found the  $\frac{\bar{U}}{\bar{R}}$  across  
259 the 72 sites is  $2.71 \pm 1.61$ , which validates the discovery by Churkina *et al.* However, the  $\frac{\bar{U}}{\bar{R}}$   
260 varied among biomes ( $2.86 \pm 1.56$  for forest,  $2.16 \pm 1.14$  for grassland,  $3.47 \pm 1.98$  for cropland,  
261  $2.89 \pm 1.47$  for wetland,  $1.89 \pm 1.10$  for shrub,  $1.83 \pm 0.88$  for savanna). This spatial convergence  
262 of  $\frac{\bar{U}}{\bar{R}}$  at the ecosystem level provides important constraints for global models that simulate  
263 various physiological processes (Peng et al., 2015; Xia et al., 2017). These findings imply that  
264 the phenology changes will greatly affect the locations of the terrestrial carbon sink by

265 modifying the length of carbon uptake period (Richardson et al., 2013; Keenan et al., 2014).

### 266 **4.3 The simulated local indicators from gridded products**

267 This study showed that the considerable spatial variations in mean annual NEP and  $IAV_{NEP}$  from  
268 global gridded products could also be inferred from their local indicators. The low variations of  
269  $\frac{U}{R}$  ratio in CLM4.5 could be largely due to their simple representations of the diverse terrestrial  
270 plant communities into a few plant functional types with parameterized properties (Cui et al.,  
271 2019; Sakschewski et al., 2015). In addition, the higher  $\frac{U}{R}$  ratio from FLUXCOM product  
272 indicated its widely reported larger net C uptake (Fig. 6) (Jung et al., 2020). Meanwhile, the  
273 ignorance of fire, land-use change and other disturbances could lead to the smaller  $\beta$  by allowing  
274 for only limited variations of phenological and physiological dynamics (Reichstein et al., 2014;  
275 Kunstler et al., 2016). Although the magnitude of  $IAV_{NEP}$  depends on the spatial resolution  
276 (Marcolla et al., 2017), we recommend future model benchmarking analyses to use not only the  
277 global product compiled from machine-learning method (Bonan et al., 2018) but also the site-  
278 level measurements or indicators (Xia et al., 2020).

### 279 **4.4 Conclusions and further implications**

280 In summary, this study highlights the changes in NEP and  $IAV_{NEP}$  over space on the land, and  
281 provides the  $\frac{U}{R}$  ratio and  $\beta$  as two simple local indicators for their spatial variations. These  
282 indicators could be helpful for locating the persistent terrestrial C sinks in where the  $\ln(\frac{U}{R})$   
283 ratio is high but the  $\beta$  is low. Their estimates based on observations are also valuable for  
284 benchmarking and improving the simulation of land-atmospheric C exchanges in Earth system  
285 models. The findings in this study have some important implications for understanding the  
286 variation of NEP on the land. First, forest ecosystems have the largest annual NEP due to the  
287 largest  $\ln(\frac{U}{R})$  while croplands show the highest  $IAV_{NEP}$  because of the highest  $\beta$ . Second, the  
288 spatial convergence of  $\frac{\bar{U}}{\bar{R}}$  suggests a tight linkage between plant growth and the non-growing  
289 season soil microbial activities (Xia et al., 2014; Zhao et al., 2016). However, it remains unclear  
290 whether the inter-biome variation in  $\frac{\bar{U}}{\bar{R}}$  is due to different plant-microbe interactions between

291 biomes. Third, the within-site convergent but spatially varying  $\beta$  needs better understanding.  
292 Previous studies have shown that a rising standard deviation of ecosystem functions could  
293 indicate an impending ecological state transition (Carpenter and Brock, 2006; Scheffer et al.,  
294 2009). Thus, a sudden shift of the  $\beta$ -value may be an important early-warning signal for the  
295 critical transition of carbon uptake sensitivity of an ecosystem. In this study, the atmospheric  
296 inversion product shows low correlation between NEP and  $\ln\left(\frac{U}{R}\right)$  in some boreal ecosystems,  
297 which might due to that the atmospheric inversion product is failed to capture the carbon uptake  
298 sensitivity in these boreal ecosystems or these boreal ecosystems are experiencing serious  
299 disturbances. Therefore, the robustness in relationship between annual NEP and  $\ln\left(\frac{U}{R}\right)$   
300 depends on the temporal stability of carbon uptake sensitivity for an ecosystem. In addition, the  
301 spatial variation in  $\beta$  reveals the differences of carbon uptake sensitivity across ecosystems.  
302 Furthermore, considering the limited eddy-covariance sites with long-term observations, these  
303 findings need further validation once the longer time-series of measurements from more sites  
304 and vegetation types become available.

### 305 **Acknowledgements**

306 This work was financially supported by the National Key R&D Program of China  
307 (2017YFA0604600), National Natural Science Foundation of China (31722009, 41630528) and  
308 National 1000 Young Talents Program of China. This work used eddy covariance dataset  
309 acquired and shared by the FLUXNET community, including these networks: AmeriFlux,  
310 AfriFlux, AsiaFlux, CarboAfrica, CarboEuropeIP, CarboItaly, CarboMont, ChinaFlux, Fluxnet-  
311 Canada, GreenGrass, ICOS, KoFlux, LBA, NECC, OzFlux-TERN, TCOS-Siberia, and USCCC.  
312 The ERA-Interim reanalysis data are provided by ECMWF and processed by LSCE. The  
313 FLUXNET eddy covariance data processing and harmonization was carried out by the European  
314 Fluxes Database Cluster, AmeriFlux Management Project, and Fluxdata project of FLUXNET,  
315 with the support of CDIAC and ICOS Ecosystem Thematic Center, and the OzFlux, ChinaFlux  
316 and AsiaFlux offices.

317 *Data availability statement.* Eddy flux data are available at  
318 <http://fluxnet.fluxdata.org/data/fluxnet2015-dataset/>; the data supporting the findings of this

319 study are available within the article and the Supplementary Information.

320 *Author contribution.* E. Cui and J. Xia devised and conducted the analysis. Y. Luo, S. Niu, Y.

321 Wang and C. Bian provided critical feedback on the method and results. All authors contributed

322 to discussion of results and writing the paper.

323 *Competing interests.* The authors declare that there is no conflict of interest.

324 **FIGURES**

325 **Figure 1** Relationship between annual NEP and  $\frac{U}{R}$  for 72 FLUXNET sites (of the form NEP =  
326  $\beta \cdot \ln\left(\frac{U}{R}\right)$ ). a, Dependence of annual NEP on the ratio between total CO<sub>2</sub> exchanges during net  
327 uptake ( $U$ ) and release ( $R$ ) periods (i.e.,  $\frac{U}{R}$ ). Each line represents one flux site with at least 5  
328 years of observations. b, Conceptual figure for the decomposition framework introduced in this  
329 study. Annual NEP can be quantitatively decomposed into the following indicators:  $NEP =$   
330  $U - R$ . c, Distribution of the explanation of  $\frac{U}{R}$  on temporal variability of NEP ( $R^2$ ) for  
331 FLUXNET sites.

332 **Figure 2** Relationship between annual NEP and  $\frac{U}{R}$  for Jena Inversion product (of the form  
333  $NEP = \beta \cdot \ln\left(\frac{U}{R}\right)$ ). The black box indicates the location of the sample.

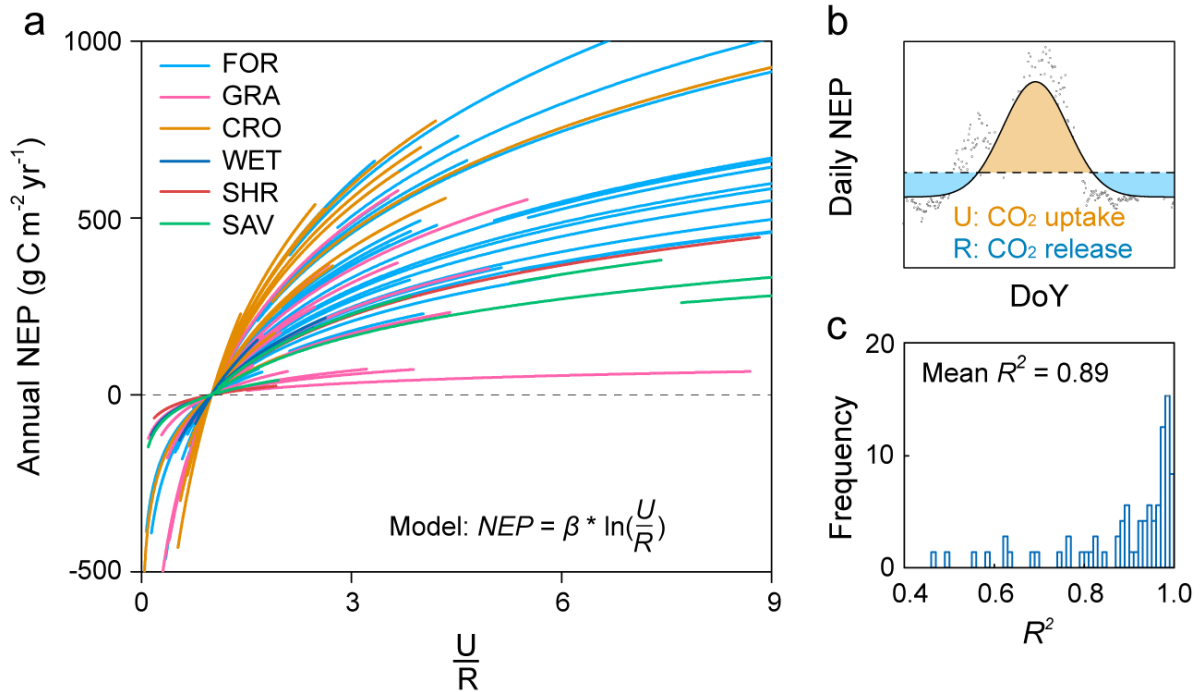
334 **Figure 3** Contributions of the two indicators in explaining the spatial patterns of mean annual  
335 NEP and  $IAV_{NEP}$ . a, The relationship between annual mean NEP and  $\ln\left(\frac{U}{R}\right)$  across FLUXNET  
336 sites ( $R^2 = 0.65, P < 0.01$ ). The insets show the variation of  $\ln\left(\frac{U}{R}\right)$  for different terrestrial  
337 biomes. b, The explanation of  $\beta$  on  $IAV_{NEP}$  ( $R^2 = 0.39, P < 0.01$ ). The insets show the distribution  
338 of parameter  $\beta$  for different terrestrial biomes. The number of site-years at each site is indicated  
339 with the size of the point.

340 **Figure 4** The linear regression between  $\frac{U}{R}$  with  $\frac{CUP}{CRP}$  ( $R^2 = 0.71, P < 0.01$ ) and  $\frac{\bar{U}}{\bar{R}}$  ( $R^2 = 0.09,$   
341  $P < 0.01$ ) across sites. The insets show the relative contributions of each indicator to the spatial  
342 variation of  $\frac{U}{R}$ . The number of site-years at each site is indicated with the size of the point.

343 **Figure 5** Representations of the spatially varying NEP and its local indicators in FLUXCOM  
344 product and the Community Land Model (CLM4.5) at the FLUXNET site level. a, The variation  
345 of mean annual NEP and  $IAV_{NEP}$  derives from FLUXNET, FLUXCOM and CLM4.5. Variation  
346 in mean annual NEP: the standard deviation of mean annual NEP across sites; Variation in  
347  $IAV_{NEP}$ : the standard deviation of  $IAV_{NEP}$  across sites. b, Representations of the local indicators  
348 for NEP in FLUXNET, FLUXCOM and CLM4.5. The corresponding distributions of  $\ln\left(\frac{U}{R}\right)$   
349 and  $\beta$  are shown at the top and right. Significance of the relationship between annual NEP and

350  $\ln\left(\frac{U}{R}\right)$  for each site is indicated by the circle: closed circles:  $P < 0.05$ ; open circles:  $P > 0.05$ . Note  
351 that the modeled results are from the pixels extracted from the same locations of the flux tower  
352 sites.

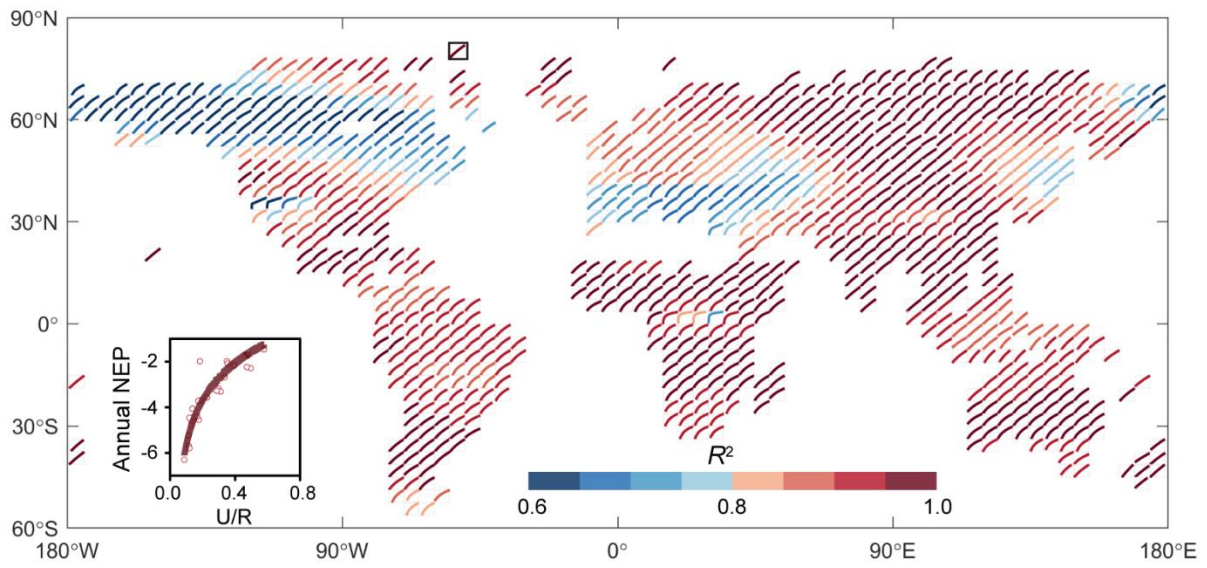
353 **Figure 6** Representations of the spatially varying NEP and its local indicators in FLUXCOM  
354 product and the Community Land Model (CLM4.5) at the global scale. a, The variation of mean  
355 annual NEP and  $I_{AV_{NEP}}$  derives from Jena Inversion, FLUXCOM and CLM4.5. Variation in  
356 mean annual NEP: the spatial variation of mean annual NEP; Variation in  $I_{AV_{NEP}}$ : the spatial  
357 variation of standard deviation in  $I_{AV_{NEP}}$ . b, Representations of the local indicators for NEP in  
358 Jena Inversion, FLUXCOM and CLM4.5.  
359



360  
 361 **Figure 1** Relationship between annual NEP and  $\frac{U}{R}$  for 72 FLUXNET sites (of the form  $NEP =$   
 362  $\beta \cdot \ln\left(\frac{U}{R}\right)$ ). **a**, Dependence of annual NEP on the ratio between total CO<sub>2</sub> exchanges during net  
 363 uptake ( $U$ ) and release ( $R$ ) periods (i.e.,  $\frac{U}{R}$ ). Each line represents one flux site with at least 5  
 364 years of data. **b**, Conceptual figure for the decomposition framework introduced in this study.  
 365 Annual NEP can be quantitatively decomposed into the following indicators:  $NEP = U - R$ . **c**,  
 366 Distribution of the explanation of  $\frac{U}{R}$  on temporal variability of FLUXNET NEP ( $R^2$ ) for  
 367 FLUXNET sites.

368



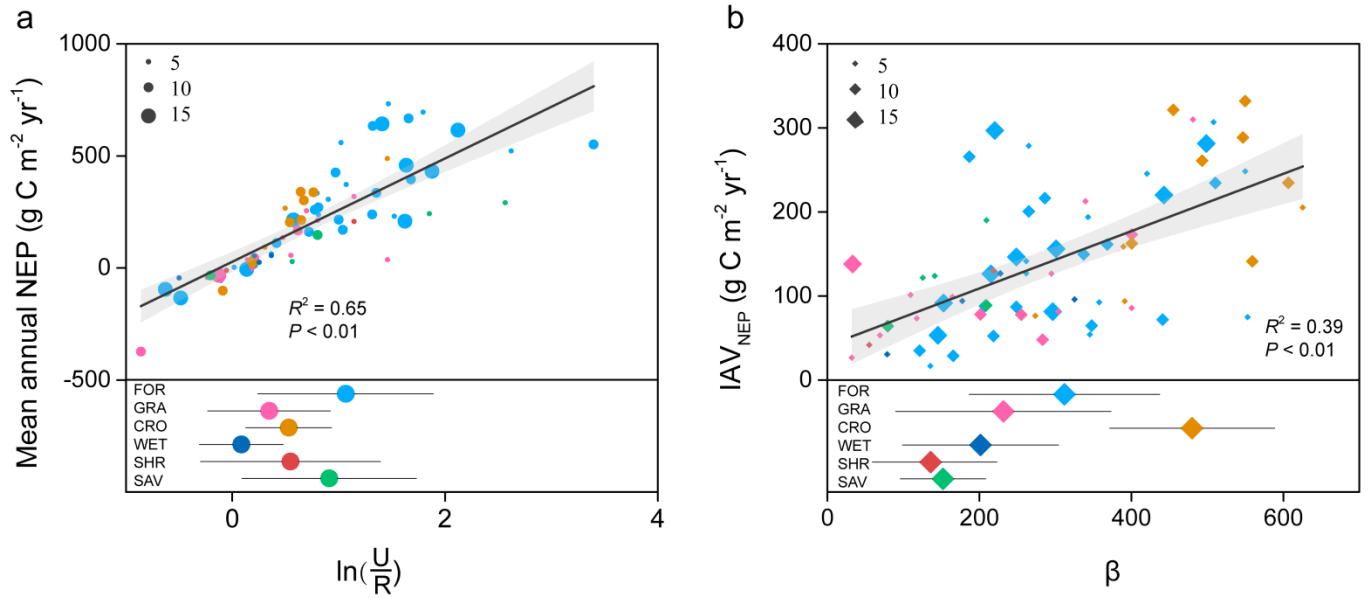


369

370 **Figure 2** Relationship between annual NEP and  $\frac{U}{R}$  for Jena Inversion product (of the form

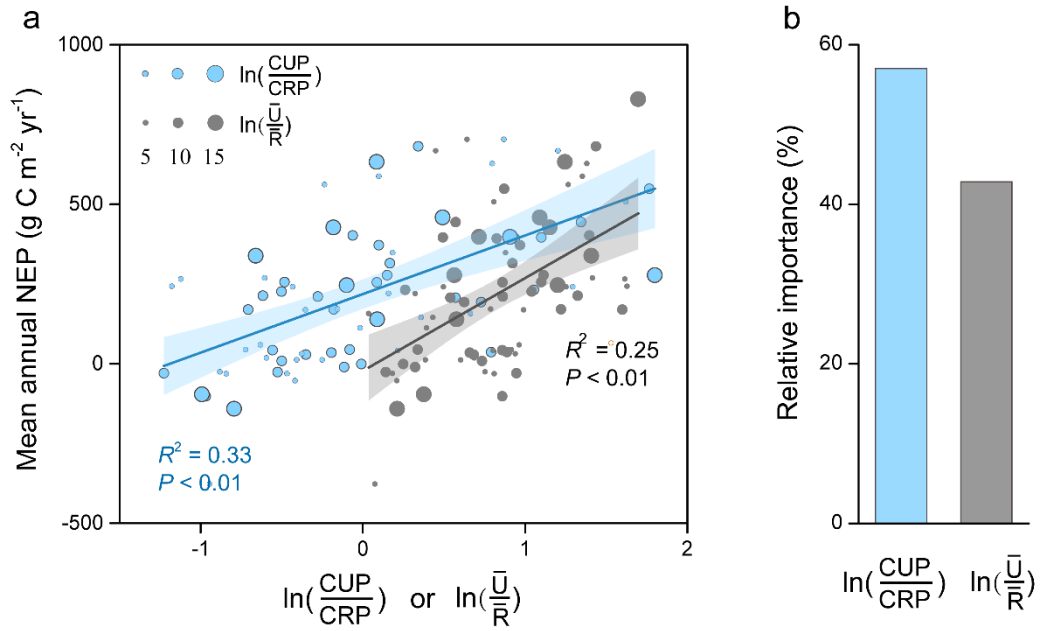
371  $NEP = \beta \cdot \ln\left(\frac{U}{R}\right)$ ). The black box indicates the location of the sample.

372

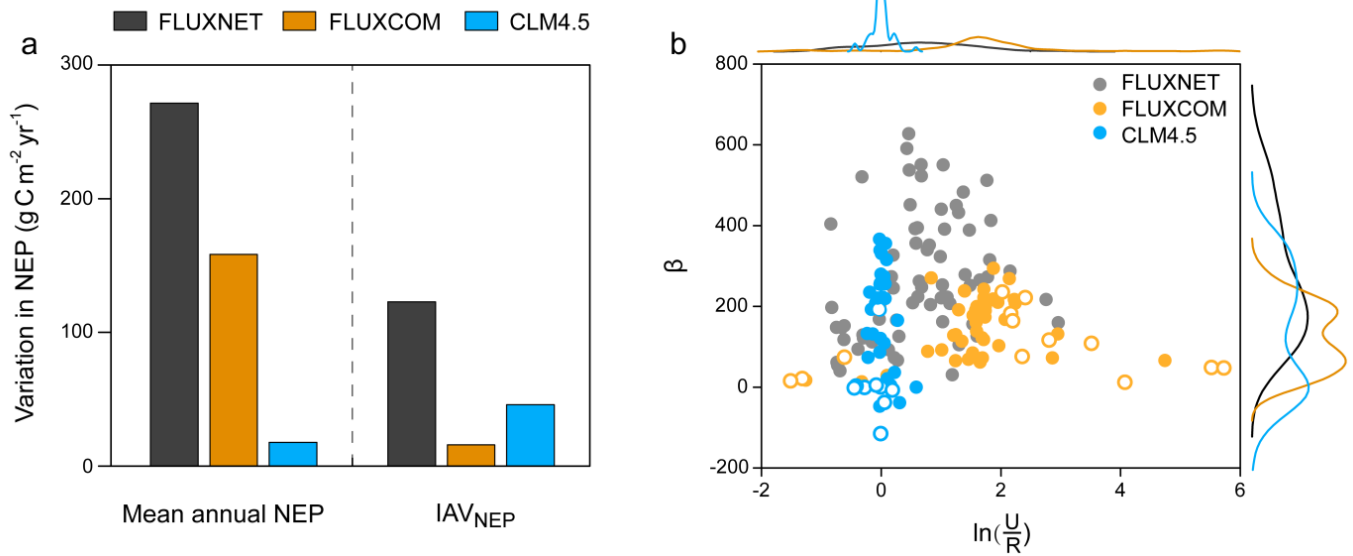


373  
 374 **Figure 3** Contributions of the two indicators in explaining the spatial patterns of mean annual  
 375 NEP and IAV<sub>NEP</sub>. **a**, The relationship between annual mean NEP and  $\ln(\frac{U}{R})$  across FLUXNET  
 376 sites ( $R^2 = 0.65$ ,  $P < 0.01$ ). The insets show the variation of  $\ln(\frac{U}{R})$  for different terrestrial  
 377 biomes. **b**, The explanation of  $\beta$  on IAV<sub>NEP</sub> ( $R^2 = 0.39$ ,  $P < 0.01$ ). The insets show the distribution  
 378 of parameter  $\beta$  for different terrestrial biomes. The number of site-years at each site is indicated  
 379 with the size of the point.

380



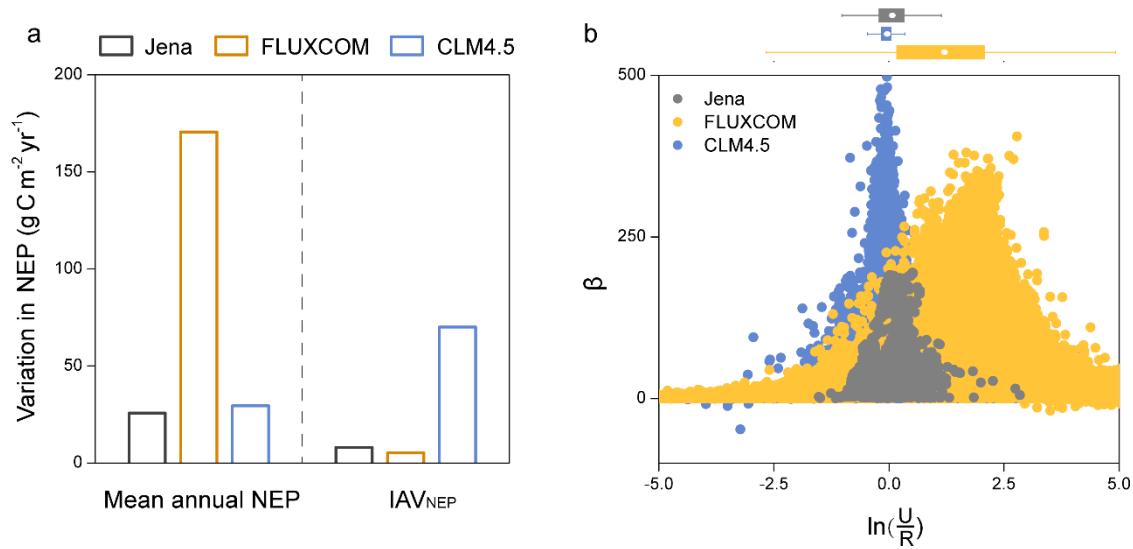
381  
 382 **Figure 4** The relative contributions of the local indicators in explaining the spatial patterns of  
 383 mean annual NEP. **a**, The linear regression between mean annual NEP with  $\frac{CUP}{CRP}$  ( $R^2 = 0.33$ ,  $P$   
 384  $< 0.01$ ) and  $\frac{\bar{U}}{\bar{R}}$  ( $R^2 = 0.25$ ,  $P < 0.01$ ) across sites. **b**, The relative contributions of each indicator  
 385 to the spatial variation of NEP. The number of site-years at each site is indicated with the size  
 386 of the point.  
 387



388

389 **Figure 5** Representations of the spatially varying NEP and its local indicators in FLUXCOM  
 390 product and the Community Land Model (CLM4.5) at the FLUXNET site level. **a**, The variation  
 391 of mean annual NEP and IAV<sub>NEP</sub> derives from FLUXNET, FLUXCOM and CLM4.5. Variation  
 392 in mean annual NEP: the standard deviation of mean annual NEP across sites; Variation in  
 393 IAV<sub>NEP</sub>: the standard deviation of IAV<sub>NEP</sub> across sites. **b**, Representations of the local indicators  
 394 for NEP in FLUXNET, FLUXCOM and CLM4.5. The corresponding distributions of  $\ln\left(\frac{U}{R}\right)$   
 395 and  $\beta$  are shown at the top and right. Significance of the relationship between annual NEP and  
 396  $\ln\left(\frac{U}{R}\right)$  for each site is indicated by the circle: closed circles:  $P < 0.05$ ; open circles:  $P > 0.05$ .  
 397 Note that the modeled results are from the pixels extracted from the same locations of the flux  
 398 tower sites.

399



400  
 401 **Figure 6** Representations of the spatially varying NEP and its local indicators in FLUXCOM  
 402 product and the Community Land Model (CLM4.5) at the global scale. a, The variation of mean  
 403 annual NEP and IAV<sub>NEP</sub> derives from Jena Inversion, FLUXCOM and CLM4.5. Variation in  
 404 mean annual NEP: the spatial variation of mean annual NEP; Variation in IAV<sub>NEP</sub>: the spatial  
 405 variation of standard deviation in IAV<sub>NEP</sub>. b, Representations of the local indicators for NEP in  
 406 Jena Inversion, FLUXCOM and CLM4.5.

407

408 **References**

- 409 Ahlström, A., Raupach, M. R., Schurgers, G., Smith, B., Arneeth, A., Jung, M., Reichstein, M.,  
410 Canadell, J. G., Friedlingstein, P., Jain, A. K., Kato, E., Poulter, B., Sitch, S., Stocker, B.  
411 D., Viovy, N., Wang, Y., Wiltshire, A., Zaehle, S., and Zeng, N.: The dominant role of semi-  
412 arid ecosystems in the trend and variability of the land CO<sub>2</sub> sink. *Science*, 348, 895-899,  
413 2015.
- 414 Arora, V. K., Katavouta, A., Williams, R. G., Jones, C. D., Brovkin, V., Friedlingstein, P.,  
415 Schwinger, J., Bopp, L., Boucher, O., Cadule, P., Chamberlain, M. A., Christian, J. R.,  
416 Delire, C., Fisher, R. A., Hajima, T., Ilyina, T., Joetzjer, E., Kawamiya, M., Koven, C.,  
417 Krasting, J., Law, R. M., Lawrence, D. M., Lenton, A., Lindsay, K., Pongratz, J., Raddatz,  
418 T., Séférian, R., Tachiiri, K., Tjiputra, J. F., Wiltshire, A., Wu, T., and Ziehn, T.: Carbon-  
419 concentration and carbon-climate feedbacks in CMIP6 models, and their comparison to  
420 CMIP5 models, *Biogeosciences Discuss.*, <https://doi.org/10.5194/bg-2019-473>, in review,  
421 2019.
- 422 Baldocchi, D., Chu, H., and Reichstein, M.: Inter-annual variability of net and gross ecosystem  
423 carbon fluxes: A review. *Agric. For. Meteorol.*, 249, 520-533, 2018.
- 424 Baldocchi, D., Sturtevant, C., and Contributors, F.: Does day and night sampling reduce spurious  
425 correlation between canopy photosynthesis and ecosystem respiration? *Agric. For.*  
426 *Meteorol.*, 207, 117-126, 2015.
- 427 Besnard, S., Carvalhais, N., Arain, A., Black, A., de Bruin, S., Buchmann, N., Cescatti, A., Chen,  
428 J., J.Clevers, J.G.P.W., Desai, A.R., Gough, C.M., Havrankova, K., Herold, M., Hörtnagl,  
429 L., Jung, M., Knohl, A., Kruijt, B., Krupkova, L., Law, B.E., Lindroth, A., Noormets, A.,  
430 Roupsard, O., Steinbrecher, R., Varlagin, A., Vincke, C. and Reichstein, M.: Quantifying  
431 the effect of forest age in annual net forest carbon balance. *Environ. Res. Lett.*, 13, 124018,  
432 2018.
- 433 Biederman, J. A., Scott, R. L., Goulden, M. L., Vargas, R., Litvak, M. E., Kolb, T. E., Yopez, E.  
434 A., Oechel, W. C., Blanken, P. D., Bell, T. W., Garatuza-Payan, J., Maurer, . E., Dore, S.,  
435 and Burns, S. P.: Terrestrial carbon balance in a drier world: the effects of water availability  
436 in southwestern North America. *Glob. Change Biol.*, 22, 1867-1879, 2016.
- 437 Bonan, G. B., Patton, E. G., Harman, I. N., Oleson, K. W., Finnigan, J. J., Lu, Y., and Burakowski,  
438 E. A.: Modeling canopy-induced turbulence in the Earth system: a unified parameterization  
439 of turbulent exchange within plant canopies and the roughness sublayer (CLM-ml v0).  
440 *Geosci. Model Dev.*, 11, 1467-1496, 2018.
- 441 Carpenter, S. R., and Brock, W. A.: Rising variance: a leading indicator of ecological transition.  
442 *Ecol. Lett.*, 9, 311-318, 2006.
- 443 Churkina, G., Schimel, D., Braswell, B. H., and Xiao, X.: Spatial analysis of growing season  
444 length control over net ecosystem exchange. *Glob. Change Biol.*, 11, 1777-1787, 2005.

445 Ciais, P., Tan, J., Wang, X., Roedenbeck, C., Chevallier, F., Piao, S. L., Moriarty, R., Broquet,  
446 G., Le Quéré, C., Canadell, J. G., Peng, S., Poulter, B., Liu Z., and Tans, P.: Five decades  
447 of northern land carbon uptake revealed by the interhemispheric CO<sub>2</sub> gradient. *Nature*, 568,  
448 221-225, 2019.

449 Cui, E., Huang, K., Arain, M. A., Fisher, J. B., Huntzinger, D. N., Ito, A., Luo, Y., Jain, A. K.,  
450 Mao, J., Michalak, A. M., Niu, S., Parazoo, N. C., Peng, C., Peng, S., Poulter, B., Ricciuto,  
451 D. M., Schaefer, K. M., Schwalm, C. R., Shi, X., Tian, H., Wang, W., Wang, J., Wei, Y.,  
452 Yan, E., Yan, L., Zeng, N., Zhu, Q., & Xia, J.: Vegetation functional properties determine  
453 uncertainty of simulated ecosystem productivity: A traceability analysis in the East Asian  
454 monsoon region. *Global Biogeochem. Cy.*, 33, 668-689, 2019.

455 Fu, Z., Dong, J., Zhou, Y., Stoy, P. C., and Niu, S.: Long term trend and interannual variability  
456 of land carbon uptake-the attribution and processes. *Environ. Res. Lett.*, 12, 014018, 2017.

457 Fu, Z., Stoy, P. C., Poulter, B., Gerken, T., Zhang, Z., Wakkulcho, G., and Niu, S.: Maximum  
458 carbon uptake rate dominates the interannual variability of global net ecosystem exchange.  
459 *Glob. Change Biol.*, 25, 3381-3394, 2019.

460 Gilmanov, T. G., Tieszen, L. L., Wylie, B. K., Flanagan, L. B., Frank, A. B., Haferkamp, M. R.,  
461 Meyers, T. P., and Morgan, J. A.: Integration of CO<sub>2</sub> flux and remotely-sensed data for  
462 primary production and ecosystem respiration analyses in the Northern Great Plains:  
463 Potential for quantitative spatial extrapolation. *Global Ecol. Biogeogr.*, 14, 271-292, 2005.

464 Gray, J. M., Frohling, S., Kort, E. A., Ray, D. K., Kucharik, C. J., Ramankutty, N., and Friedl,  
465 M. A.: Direct human influence on atmospheric CO<sub>2</sub> seasonality from increased cropland  
466 productivity. *Nature*, 515, 398-401, 2014.

467 Grömping, U.: Estimators of relative importance in linear regression based on variance  
468 decomposition. *Am. Stat.*, 61, 139-147, 2007.

469 Huang, K., Xia, J., Wang, Y., Ahlström, A., Chen, J., Cook, R. B., Cui, E., Fang, Y., Fisher, J. B.,  
470 Huntzinger, D. N., Li, Z., Michalak, A. M., Qiao, Y., Schaefer, K., Schwalm, C., Wang, J.,  
471 Wei, Y., Xu, X., Yan, L., Bian C., and Luo, Y.: Enhanced peak growth of global vegetation  
472 and its key mechanisms. *Nat. Ecol. Evol.*, 2, 1897-1905, 2018.

473 Jung, M., Reichstein, M., Schwalm, C. R., Huntingford, C., Sitch, S., Ahlström, A., Arneeth, A.,  
474 Camps-Valls, G., Ciais, P., Friedlingstein, P., Gans, F., Ichii, K., Jain, A. K., Kato, E., Papale,  
475 D., Poulter, B., Raduly, B., Rödenbeck, C., Tramontana, G., Viovy, N., Wang, Y., Weber,  
476 U., Zaehle S., and Zeng, N.: Compensatory water effects link yearly global land CO<sub>2</sub> sink  
477 changes to temperature. *Nature*, 541, 516-520, 2017.

478 Jung, M., Schwalm, C., Migliavacca, M., Walther, S., Camps-Valls, G., Koirala, S., Anthoni, P.,  
479 Besnard, S., Bodesheim, P., Carvalhais, N., Chevallier, F., Gans, F., Goll, D. S., Haverd, V.,  
480 Köhler, P., Ichii, K., Jain, A. K., Liu, J., Lombardozzi, D., Nabel, J. E. M. S., Nelson, J. A.,  
481 O'Sullivan, M., Pallandt, M., Papale, D., Peters, W., Pongratz, J., Rödenbeck, C., Sitch, S.,  
482 Tramontana, G., Walker, A., Weber, U., and Reichstein, M.: Scaling carbon fluxes from  
483 eddy covariance sites to globe: synthesis and evaluation of the FLUXCOM approach,

484 Biogeosciences, 17, 1343-1365, 2020.

485 Keenan, T. F., Gray, J., Friedl, M. A., Toomey, M., Bohrer, G., Hollinger, D. Y., Munger, J. W.,  
486 O’Keefe, J., Schmid, H. P., Wing, I. S., Yang, B., and Richardson, A. D.: Net carbon uptake  
487 has increased through warming-induced changes in temperate forest phenology. *Nat. Clim.*  
488 *Change*, 4, 598-604, 2014.

489 Kunstler, G., Falster, D., Coomes, D. A., Hui, F., Kooyman, R. M., Laughlin, D. C., Poorter, L.,  
490 Vanderwel, M., Vieilledent, G., Wright, S. J., Aiba, M., Baraloto, C., Caspersen, J.,  
491 Cornelissen, J. H. C., Gourlet-Fleury, S., Hanewinkel, M., Herault, B., Kattge, J.,  
492 Kurokawa, H., Onoda, Y., Peñuelas, J., Poorter, H., Uriarte, M., Richardson, S., Ruiz-  
493 Benito, P., Sun, I., Ståhl, G., Swenson, N. G., Thompson, J., Westerlund, B., Wirth, C.,  
494 Zavala, M. A., Zeng, H., Zimmerman, J. K., Zimmermann N. E., and Westoby, M.: Plant  
495 functional traits have globally consistent effects on competition. *Nature*, 529, 204-207,  
496 2016.

497 Le Quéré, C., Andrew, R. M., Friedlingstein, P., Sitch, S., Hauck, J., Pongratz, J., Pickers, P. A.,  
498 Korsbakken, J. I., Peters, G. P., Canadell, J. G., Arneeth, A., Arora, V. K., Barbero, L., Bastos,  
499 A., Bopp, L., Chevallier, F., Chini, L. P., Ciais, P., Doney, S. C., Gkritzalis, T., Goll, D. S.,  
500 Harris, I., Haverd, V., Hoffman, F. M., Hoppema, M., Houghton, R. A., Hurtt, G., Ilyina,  
501 T., Jain, A. K., Johannessen, T., Jones, C. D., Kato, E., Keeling, R. F., Goldewijk, K. K.,  
502 Landschützer, P., Lefèvre, N., Lienert, S., Liu, Z., Lombardozzi, D., Metzl, N., Munro, D.  
503 R., Nabel, J. E. M. S., Nakaoka, S., Neill, C., Olsen, A., Ono, T., Patra, P., Pregon, A.,  
504 Peters, W., Peylin, P., Pfeil, B., Pierrot, D., Poulter, B., Rehder, G., Resplandy, L.,  
505 Robertson, E., Rocher, M., Rödenbeck, C., Schuster, U., Schwinger, J., Séférian, R.,  
506 Skjelvan, I., Steinhoff, T., Sutton, A., Tans, P. P., Tian, H., Tilbrook, B., Tubiello, F. N., van  
507 der Laan-Luijkx, I. T., van der Werf, G. R., Viovy, N., Walker, A. P., Wiltshire, A. J., Wright,  
508 R., Zaehle, S., and Zheng, B.: Global carbon budget 2018. *Earth Syst. Sci. Data*, 10, 405,  
509 2018.

510 Li, G., Han, H., Du, Y., Hui, D., Xia, J., Niu, S., Li, X., and Wan, S.: Effects of warming and  
511 increased precipitation on net ecosystem productivity: a long-term manipulative  
512 experiment in a semiarid grassland. *Agric. For. Meteorol.*, 232, 359-366, 2017.

513 Luo, Y., and Weng, E.: Dynamic disequilibrium of the terrestrial carbon cycle under global  
514 change. *Trends Ecol. Evol.*, 26, 96-104, 2011.

515 Luo, Y., and Zhou, X.: *Soil respiration and the environment*. Elsevier, 2006.

516 Marcolla, B., Rödenbeck, C., and Cescatti, A.: Patterns and controls of inter-annual variability  
517 in the terrestrial carbon budget. *Biogeosciences*, 14, 3815-3829, 2017.

518 Musavi, T., Migliavacca, M., Reichstein, M., Kattge, J., Wirth, C., Black, T. A., Janssens, I.,  
519 Knohl, A., Loustau, D., Roupsard, O., Varlagin, A., Rambal, S., Cescatti, A., Gianelle, D.,  
520 Kondo, H., Tamrakar, R., and Mahecha, M. D.: Stand age and species richness dampen  
521 interannual variation of ecosystem-level photosynthetic capacity. *Nat. Ecol. Evol.*, 1, 0048,  
522 2017.



523 Niu, S., Fu, Z., Luo, Y., Stoy, P. C., Keenan, T. F., Poulter, B., Zhang, L., Piao, S., Zhou, X.,  
524 Zheng, H., Han, J., Wang, Q., and Yu, G.: Interannual variability of ecosystem carbon  
525 exchange: From observation to prediction. *Global Ecol. Biogeogr.*, 26, 1225-1237, 2017.

526 Novick, K. A., Oishi, A. C., Ward, E. J., Siqueira, M. B., Juang, J. Y., and Stoy, P. C.: On the  
527 difference in the net ecosystem exchange of CO<sub>2</sub> between deciduous and evergreen forests  
528 in the southeastern United States. *Glob. Change Biol.*, 21, 827-842, 2015.

529 Oleson, K. W., Lawrence, D. M., Bonan, G. B., Drewniak, B., Huang, M., Koven, C. D., Levis,  
530 S., Li, F., Riley, W. J., Subin, Z. M., Swenson, S. C., Thornton, P. E., Bozbiyik, A., Fisher,  
531 R., Heald, C. L., Kluzek, E., Lamarque, J.-F., Lawrence, P. J., Leung, L. R., Lipscomb, W.,  
532 Muszala, S., Ricciuto, D. M., Sacks, W., Sun, Y., Tang, J., and Yang, Z.-L.: Technical  
533 description of version 4.5 of the Community Land Model (CLM), NCAR Earth System  
534 Laboratory-Climate and Global Dynamics Division, Boulder, Colorado, USA, Tech. Rep.  
535 TN-503+STR, [http://www.cesm.ucar.edu/models/cesm1.2/clm/CLM45\\_Tech\\_Note.pdf](http://www.cesm.ucar.edu/models/cesm1.2/clm/CLM45_Tech_Note.pdf)  
536 (last access: 27 September 2017), 2013.

537 Pastorello, G., Papale, D., Chu, H., Trotta, C., Agarwal, D., Canfora, E., Baldocchi, D., and Torn,  
538 M.: A new data set to keep a sharper eye on land-air exchanges. *Eos*, 98, 2017.

539 Peng, S., Ciais, P., Chevallier, F., Peylin, P., Cadule, P., Sitch, S., Piao, S., Ahlström, A.,  
540 Huntingford, C., Levy, P., Li, X., Liu, Y., Lomas, M., Poulter, B., Viovy, N., Wang, T.,  
541 Wang, X., Zaehle, S., Zeng, N., Zhao, F., and Zhao, H.: Benchmarking the seasonal cycle  
542 of CO<sub>2</sub> fluxes simulated by terrestrial ecosystem models. *Global Biogeochem. Cy.*, 29, 46-  
543 64, 2015.

544 Peylin, P., Law, R. M., Gurney, K. R., Chevallier, F., Jacobson, A. R., Maki, T., Niwa, Y., Patra,  
545 P. K., Peters, W., Rayner, P. J., Rödenbeck, C., van der Laan-Luijkx, I. T., and Zhang, X.:  
546 Global atmospheric carbon budget: results from an ensemble of atmospheric CO<sub>2</sub>  
547 inversions. *Biogeosciences*, 10, 6699-6720, 2013.

548 Poulter, B., Frank, D., Ciais, P., Myneni, R. B., Andela, N., Bi, J., Broquet, G., Canadell, J. G.,  
549 Chevallier, F., Liu, Y. Y., Running, S. W., Sitch, S., and van der Werf, G. R.: Contribution  
550 of semi-arid ecosystems to interannual variability of the global carbon cycle. *Nature*, 509,  
551 600-603, 2014.

552 Randerson, J. T.: Climate science: Global warming and tropical carbon. *Nature*, 494, 319-320,  
553 2013.

554 Randerson, J. T., Chapin III, F. S., Harden, J. W., Neff, J. C., and Harmon, M. E.: Net ecosystem  
555 production: a comprehensive measure of net carbon accumulation by ecosystems. *Ecol.*  
556 *Appl.*, 12, 937-947, 2002.

557 R Development Core Team.: R: A Language and Environment for Statistical Computing 3-  
558 900051-07-0, R Foundation for Statistical Computing, Vienna, Austria, 2011.

559 Reichstein, M., Bahn, M., Mahecha, M. D., Kattge, J., and Baldocchi, D. D.: Linking plant and  
560 ecosystem functional biogeography. *Proc. Natl Acad. Sci. USA*, 111, 13697-13702, 2014.

561 Reichstein, M., Falge, E., Baldocchi, D., Papale, D., Aubinet, M., Berbigier, P., Bernhofer, C.,

562 Buchmann, N., Gilmanov, T., Granier, A., Grünwald, T., Havránková, K., Ilvesniemi, H.,  
 563 Janous, D., Knohl, A., Laurila, T., Lohila, A., Loustau, D., Matteucci, G., Meyers, T.,  
 564 Miglietta, F., Ourcival, J., Pumpanen J., Rambal, S., Rotenberg, E., Sanz, M., Tenhunen,  
 565 J., Seufert, G., Vaccari, F., Vesala, T., Yakir, D., and Valentini, R.: On the separation of net  
 566 ecosystem exchange into assimilation and ecosystem respiration: review and improved  
 567 algorithm. *Glob. Change Biol.*, 11, 1424-1439, 2005.

568 Richardson, A. D., Keenan, T. F., Migliavacca, M., Ryu, Y., Sonnentag, O., and Toomey, M.:  
 569 Climate change, phenology, and phenological control of vegetation feedbacks to the  
 570 climate system. *Agric. For. Meteorol.*, 169, 156-173, 2013.

571 Rödenbeck, C., Zaehle, S., Keeling, R., and Heimann, M.: How does the terrestrial carbon  
 572 exchange respond to inter-annual climatic variations? *Biogeosciences*, 15, 2481-2498,  
 573 2018.

574 Sakschewski, B., von Bloh, W., Boit, A., Rammig, A., Kattge, J., Poorter, L., Peñuelas, J., and  
 575 Thonicke, K.: Leaf and stem economics spectra drive diversity of functional plant traits in  
 576 a dynamic global vegetation model. *Glob. Change Biol.*, 21, 2711-2725, 2015.

577 Scheffer, M., Bascompte, J., Brock, W. A., Brovkin, V., Carpenter, S. R., Dakos, V., Held, H.,  
 578 van Nes, E. H., Rietkerk, M., and Sugihara, G.: Early-warning signals for critical transitions.  
 579 *Nature*, 461, 53-59, 2009.

580 Valentini, R., Matteucci, G., Dolman, A. J., Schulze, E. D., Rebmann, C. J. M. E. A. G., Moors,  
 581 E. J., Granier, A., Gross, P., Jensen, N. O., Pilegaard, K., Lindroth, A., Grelle, A., Bernhofer,  
 582 C., Grünwald, T., Aubinet, M., Ceulemans, R., Kowalski, A. S., Vesala, T., Rannik, Ü.,  
 583 Berbigier, P., Loustau, D., Guðmundsson, J., Thorgeirsson, H., Ibrom, A., Morgenstern, K.,  
 584 Clement, R., Moncrieff, J., Montagnani, L., Minerbi S., and Jarvis, P. G.: Respiration as  
 585 the main determinant of carbon balance in European forests. *Nature*, 404, 861-865, 2000.

586 Von Buttlar, J., Zscheischler, J., Rammig, A., Sippel, S., Reichstein, M., Knohl, A., Jung, M.,  
 587 Menzer, O., Arain, M., Buchmann, N., Cescatti, A., Geinelle, D., Kiely, G., Law, B.,  
 588 Magliudo, V., Margolis, H., McCaughey, H., Merbold, L., Migliavacca, M., Montagnani,  
 589 L., Oechel, W., Pavelka, M., Pelchl, M., Rambal, S., Raschi, A., Scott, R.L., Vaccari, F.,  
 590 Van Gorsel, E., Varlagin, A., Wohlfahrt, G., and Mahecha, M.: Impacts of droughts and  
 591 extreme temperature events on gross primary production and ecosystem respiration: a  
 592 systematic assessment across ecosystems and climate zones. *Biogeosciences*, 15, 1293-  
 593 1318, 2017.

594 Xia, J., Chen, J., Piao, S., Ciais, P., Luo, Y., and Wan, S.: Terrestrial carbon cycle affected by  
 595 non-uniform climate warming. *Nat. Geosci.*, 7, 173-180, 2014.

596 Xia, J., McGuire, A. D., Lawrence, D., Burke, E., Chen, G., Chen, X., Delire, C., Koven, C.,  
 597 MacDougall, A., Peng, S., Rinke, A., Saito, K., Zhang, W., Alkama, R., Bohn, T. J., Ciais,  
 598 P., Decharme, B., Gouttevin, I., Hajima, T., Hayes, D. J., Huang, K., Ji, D., Krinner, G.,  
 599 Lettenmaier, D. P., Miller, P. A., Moore, J. C., Smith, B., Sueyoshi, T., Shi, Z., Yan, L.,  
 600 Liang, J., Jiang, L., Zhang, Q., and Luo, Y.: Terrestrial ecosystem model performance in

601           simulating productivity and its vulnerability to climate change in the northern permafrost  
602           region. *J. Geophys. Res-Bioge.*, 122, 430-446, 2017.

603 Xia, J., Niu, S., Ciais, P., Janssens, I. A., Chen, J., Ammann, C., Arain, A., Blanken, P. D.,  
604           Cescatti, A., Bonal, D., Buchmann, N., Curtis, P. S., Chen, S., Dong, J., Flanagan, L. B.,  
605           Frankenberg, C., Georgiadis, T., Gough, C. M., Hui, D., Kiely, G., Li, J., Lund, M.,  
606           Magliulo, V., Marcolla, B., Merbold, L., Montagnani, L., Moors, E. J., Olesen, J. E., Piao,  
607           S., Raschi, A., Rouspard, O., Suyker, A. E., Urbaniak, M., Vaccari, F. P., Varlagin, A.,  
608           Vesala, T., Wilkinson, M., Weng, E., Wohlfahrt, G., Yan, L., and Luo, Y.: Joint control of  
609           terrestrial gross primary productivity by plant phenology and physiology. *Proc. Natl Acad.*  
610           *Sci. USA*, 112, 2788-2793, 2015.

611 Xia, J., Wang, J., and Niu, S.: Research challenges and opportunities for using big data in global  
612           change biology. *Glob. Change Biol.*, 2020. <https://doi.org/10.1111/gcb.15317>

613 Yu, G., Chen, Z., Piao, S., Peng, C., Ciais, P., Wang, Q., Li, X., and Zhu, X.: High carbon dioxide  
614           uptake by subtropical forest ecosystems in the East Asian monsoon region. *Proc. Natl Acad.*  
615           *Sci. USA*, 111, 4910-4915, 2014.

616 Zeng, N., Zhao, F., Collatz, G. J., Kalnay, E., Salawitch, R. J., West, T. O., and Guanter, L.:  
617           Agricultural Green Revolution as a driver of increasing atmospheric CO<sub>2</sub> seasonal  
618           amplitude. *Nature*, 515, 394-397, 2014.

619 Zhao, J., Peichl, M., Öquist, M., and Nilsson, M. B.: Gross primary production controls the  
620           subsequent winter CO<sub>2</sub> exchange in a boreal peatland. *Glob. Change Biol.*, 22, 4028-4037,  
621           2016.

622 Zhou, S., Zhang, Y., Ciais, P., Xiao, X., Luo, Y., Caylor, K. K., Huang, Y., and Wang, G.:  
623           Dominant role of plant physiology in trend and variability of gross primary productivity in  
624           North America. *Sci. Rep.*, 7, 41366, 2017.

625